



CHORUS

This is the accepted manuscript made available via CHORUS. The article has been published as:

First-principles calculation of the elastic dipole tensor of a point defect: Application to hydrogen in α -zirconium

R. Nazarov, J. S. Majevadia, M. Patel, M. R. Wenman, D. S. Balint, J. Neugebauer, and A. P. Sutton

Phys. Rev. B **94**, 241112 — Published 21 December 2016

DOI: [10.1103/PhysRevB.94.241112](https://doi.org/10.1103/PhysRevB.94.241112)

First Principles Calculation of the Elastic Dipole Tensor of a Point Defect: Application to Hydrogen in α -Zirconium

R. Nazarov,¹ J. S. Majevadia,² M. Patel,² M. R. Wenman,³ D. S. Balint,⁴ J. Neugebauer,⁵ and A. P. Sutton^{2,*}

¹Physics Division, Lawrence Livermore National Laboratory, 7000 East Ave., Livermore CA 94550, USA

²Department of Physics, Imperial College London, Exhibition Road, London SW7 2AZ, UK.

³Department of Materials, Imperial College London, Exhibition Road, London SW7 2AZ, UK.

⁴Department of Mechanical Engineering, Imperial College London, Exhibition Road, London SW7 2AZ, UK.

⁵Max-Planck-Institut für Eisenforschung GmbH, Max-Planck Strasse, Düsseldorf 40237, Germany.

(Dated: October 17, 2016)

The elastic dipole tensor is a fundamental quantity relating the elastic field and atomic structure of a point defect. We review three methods in the literature to calculate the dipole tensor and apply them to hydrogen in α -zirconium using density functional theory (DFT). The results are compared with the dipole tensor deduced from earlier experimental measurements of the λ -tensor for hydrogen in α -zirconium. There are significant errors with all three methods. We show that calculation of the λ -tensor, in combination with experimentally measured elastic constants and lattice parameters, yields dipole tensor components that differ from experimental values by only 10–20%. There is evidence to suggest that current state-of-the-art DFT calculations underestimate bonding between hydrogen and α -zirconium.

Elastic interactions between point defects and other defects play a central role in the evolution of microstructures in materials. The simplest analysis treats the point defect as a misfitting sphere, in an elastically isotropic medium, where it interacts with the hydrostatic stress fields of other defects [1]. But there are many point defects with lower symmetry, such as split interstitials, divacancies, impurity-vacancy complexes, and small clusters of point defects where the misfitting sphere model is inaccurate. In contrast the elastic dipole tensor captures the symmetry of the point defect. It forms a bridge between the atomic structure of the defect and its long-range elastic field. For these reasons Leibfried and Breuer stated in 1982 the dipole tensor ‘is, without exaggeration, the most important ... concept needed in defect physics’ [2].

In this work we review three methods from the literature to calculate the elastic dipole tensor. We analyze the approximations made by each of them, and we apply state-of-the-art density functional theory (DFT) techniques to see whether each of them can reproduce the dipole tensor for H in α -Zr deduced from experimental measurements of the λ -tensor by MacEwen et al.[3]. As far as we know this is the first comparison between dipole tensor components deduced from experimental measurements of the λ -tensor and calculations from first principles. We find significant disagreement and discuss possible sources of error in the calculations and experimental measurements.

α -Zr alloys are used extensively in water-cooled nuclear reactors for fuel cladding. Delayed hydride cracking [4] in these alloys is an important phenomenon arising from elastic interactions involving H point defects. H is

produced primarily by a corrosion reaction and enters the metal where it is attracted to cracks and notches by their elastic fields. H occupies tetrahedral interstitial sites in the hexagonal close packed (hcp) crystal structure of α -Zr [5, 6] where it forms three equivalent bonds to Zr-atoms in the basal plane and a fourth non-equivalent bond along the c-axis (see Fig.1 in the Supplemental Material). Therefore the defect has trigonal symmetry, which directly affects its interaction with cracks and notches, and hence its diffusion in their stress fields.

To determine the elastic dipole tensor of a point defect we assume the defect is in an equilibrium position in the host crystal. Let $\mathbf{f}^{m/q}$ be the force that atom m exerts on atom q in this equilibrium state, the locations of which are \mathbf{m} and \mathbf{q} . Since the system is in equilibrium the total force acting on atom q , $\sum_m \mathbf{f}^{m/q}$ is zero. Following Stoneham [8] we call the forces $\mathbf{f}^{m/q}$ *defect forces*. Consider the change in total energy when the atoms are displaced from their equilibrium positions by an infinitesimal amount:

$$\delta E = -\frac{1}{2} \sum_m \sum_{q \neq m} f_k^{m/q} \delta(q_k - m_k), \quad (1)$$

where the summation on k is implied, and the factor $\frac{1}{2}$ is to correct for the double counting of each interaction. It follows that if e^h is an infinitesimal, *homogeneous* strain, such that $\delta(q_k - m_k) = e_{kj}^h (q_j - m_j)$ the change in energy is as follows:

$$\delta E = -V \left\{ \frac{1}{2V} \sum_m \sum_{q \neq m} f_k^{m/q} (q_j - m_j) \right\} e_{kj}^h, \quad (2)$$

where V is the total volume occupied by atoms in the sum over m . Using $\delta E = -V \langle \sigma_{kj} \rangle e_{kj}^h$ we recognise the term in braces as the average stress $\langle \sigma_{kj} \rangle$ in volume V .

* Corresponding author: a.sutton@imperial.ac.uk

Consider a periodic supercell containing a point defect d at \mathbf{d} . Both sums in Eq. (2) are taken over all atoms in the supercell, and V is now the volume of the supercell. We may rewrite $\langle \sigma_{kj} \rangle$ as follows:

$$\langle \sigma_{kj} \rangle = p_{kj}/V + s_{kj}, \quad (3)$$

where the first term on the right involves the dipole tensor p_{kj} in the form suggested by Gillan [7]:

$$p_{kj} = \sum_{m \neq d} f_k^{m/d} (d_j - m_j), \quad (4)$$

If the defect forces, $\mathbf{f}^{m/d}$, can be evaluated this expression provides a route to calculate the dipole tensor, which we call the *defect forces method*. Expressions for the total force on a given atom in some models of interatomic forces do indeed comprise a sum of forces exerted by its neighbors. Examples include pair potentials, embedded atom potentials and tight binding models, and Eq. (4) may then be applied directly. But in many other cases, including DFT with a plane wave basis, the total force on an atom is not expressible as a sum of contributions from neighboring atoms. Nevertheless, the force exerted by each neighbor on a host or impurity atom d can always be calculated by the following procedure. Once the total force on each atom has been brought to zero, atom d is removed from the system while the positions of all other atoms are fixed. The remaining electrons are then made self-consistent with the new potential, while still keeping all nuclei fixed. Each neighboring atom now experiences a net force. That net force must be equal and opposite to the force the neighbor exerted on atom d when atom d was present.

The second term on the right of Eq. (3) arises from atomic interactions not involving atom d :

$$s_{kj} = \frac{1}{2V} \sum_{m \neq d} \sum_{q \neq m, d} f_k^{m/q} (q_j - m_j), \quad (5)$$

This term represents the contribution to the average stress in the supercell arising from interactions between host atoms only. In Eq. (4) this term is neglected because it is assumed only the defect atom is a source of stress. But interactions between surrounding host atoms may be altered by the defect atom through 3-body and higher order interactions. The affected host atoms then become part of the point defect, contributing to the stress it generates. This is particularly clear with small self-interstitial clusters where the distinction between host and defect atoms is often untenable.

Since in general the distinction between host and defect atoms cannot be maintained the *stress method* is based on the following expression [9, 36–38]:

$$p_{kj} = V \left(\frac{\partial E}{\partial e_{kj}^h} \right)_{e_{kj}^h=0} = V \langle \sigma_{kj} \rangle. \quad (6)$$

The derivative in Eq. (6) is evaluated numerically by applying small strains to the supercell and calculating the changes in the total energy. Following the application of each small, but finite, homogeneous strain to the supercell the forces on all atoms are relaxed.

The average stress $\langle \sigma_{ij} \rangle$ in the supercell may be relaxed by allowing the supercell vectors to change, which strains the supercell by e_{kl}^h . The forces on all atoms are relaxed when the supercell vectors are changed. Assuming the concentration of point defects is sufficiently small that the elastic constants of the material are unchanged, the total elastic energy of the supercell then becomes:

$$E_{\text{el}} = -p_{ij} e_{ij}^h + \frac{V}{2} c_{ijkl} e_{ij}^h e_{kl}^h. \quad (7)$$

Minimizing this elastic energy leads to the *strain method* [9] of determining the dipole tensor:

$$p_{ij} = V c_{ijkl} \epsilon_{kl}^h, \quad (8)$$

where ϵ_{kl}^h is the homogeneous strain for which $\partial E_{\text{el}} / \partial e_{ij}^h = 0$.

In summary, the defect forces method Eq. (4), the stress method Eq. (6) and the strain method Eq. (8) are based on different assumptions. In principle the stress and strain methods should agree in the limit of infinitely large supercells. Different numerical errors may be expected with each method. In the present case an H atom is assumed to occupy a tetrahedral site in α -Zr. We will assess the accuracy of each method by comparing its prediction for H in α -Zr with experimental measurements.

MacEwen *et al.* [3] measured changes in the lattice parameters in α -Zr as a function of interstitial deuterium concentration, at temperatures between 727 K and 777 K, using time of flight neutron diffraction. The λ -tensor is defined by $\lambda_{ij} = d\epsilon_{ij}/dC_D$, where C_D is the atomic fraction of D-atoms, and ϵ_{ij} is the eigenstrain tensor caused by D-atoms. They obtained: $\lambda_{11} = 0.033$ and $\lambda_{33} = 0.054$.

As shown by Nowick and Berry [10] the λ -tensor and the dipole tensor are related:

$$p_{ij} = \Omega_{\text{Zr}} c_{ijkl} \lambda_{kl}, \quad (9)$$

where Ω_{Zr} is the atomic volume of α -Zr. It is assumed that the elastic constants of the alloy are the same as those of α -Zr. In the Supplemental Material we derive Eq. (9) and obtain the following dipole tensor components for H in α -Zr at $T = 0$ K: $p_{11} = 1.57$ eV and $p_{33} = 1.96$ eV.

To calculate the dipole tensor of H in α -Zr we use DFT, as implemented in VASP [11], employing either the local density approximation (LDA) [12, 13] or the Perdew-Burke-Ernzerhof (PBE) generalized gradient approximation [14]. For Zr the semi-core 4s and 4p states are treated as valence states, together with the 5s and 4d

states in a projector augmented wave (PAW) pseudopotential [15, 16] with an outermost core radius of 2.5 au. A standard PAW pseudopotential in VASP is used for H with an outermost core radius of 1.1 au. The plane-wave energy cutoff is 400 eV. Fermi-surface smearing is implemented using the second-order Methfessel-Paxton (MP) method [17] with a smearing width of 0.1 eV. The atomic relaxations caused by the H-atom are deemed complete when the maximum force on any atom is less than 1 meV/Å. The charge density is considered consistent with the Kohn-Sham potential when the total electronic energy changes by less than 10^{-7} eV between successive iterations.

Supercells of 96, 150, 200, 288 and 392 Zr-atoms and 1 H-atom in a tetrahedral interstitial site are used with periodic boundary conditions applied in all directions. The real space supercells and the Γ -centered Monkhorst-Pack [18] \mathbf{k} -point grids for each supercell are given in Table I. Lattice parameters and elastic constants vary slightly with the supercell size owing to small differences in the \mathbf{k} -point sampling and other numerical errors.

The enthalpy of solution ΔH_H is calculated as the total energy of an H-containing supercell, minus the sum of the total energy of the pure α -Zr supercell and half the energy of an H_2 molecule. It includes the difference, -0.01 eV, between the zero-point energy for an H-atom in a tetrahedral site in α -Zr and half the zero-point energy of an H_2 molecule. The zero-point energies are obtained by solving the three-dimensional Schrödinger equation, as described in the work of Nazarov *et al.* [19].

The volume of formation, Ω_H , of interstitial H is calculated as the volume of the supercell containing H with supercell vectors that minimize the total energy minus the total volume of the pure α -Zr supercell. ΔH_H and Ω_H are compared to experimental measurements in Table I.

The dipole tensor in Eq. (4) is evaluated using the relaxed defect forces and the relaxed positions of the Zr atoms relative to the H-interstitial, taking care to ensure that complete shells of neighbors are included. Assuming the residual forces on the N_{at} atoms are randomly distributed we calculate their standard deviation σ_f . An estimate of the error in p_{ij} is then $\sigma_f \sum_n |n_j - d_j|$ eV, which increases with the volume of the supercell. It is vital that the tolerance on the maximum force experienced by any atom in the relaxation is as small as possible.

To implement the stress and strain methods a potential energy surface (PES) is constructed by applying homogeneous strains to each supercell containing the H-atom of $-0.01, -0.005, 0, 0.005, 0.01$ biaxially in the basal plane, and independent strains of $-0.01, -0.005, 0, 0.005, 0.01$ normal to the basal plane. At each of these 25 configurations the total energy is calculated, following relaxation of all atomic forces in the supercell. These energies are fitted to a paraboloid using the method of least squares.

The stress method is to evaluate the derivatives of

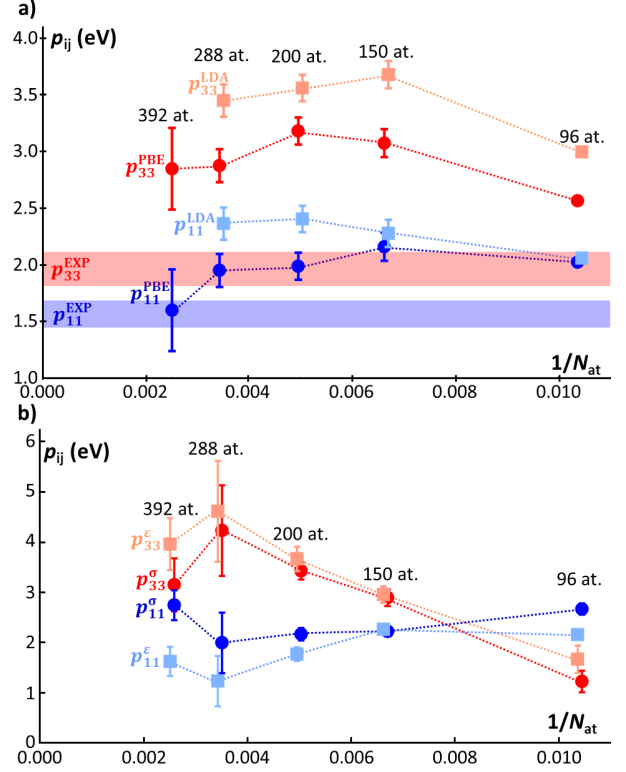


FIG. 1: (a) Elastic dipole tensor components, as computed by the defect forces method, plotted against the inverse of the number, N_{at} , of Zr-atoms in the supercell. Circles show PBE results, squares show LDA results. Components of the dipole tensor derived from experimental results are shown by horizontal bands, the widths of which indicate their errors. Red symbols show p_{33} , and blue show p_{11} . (b) Elastic dipole tensor components, as computed by the stress (σ superscript) and strain (ϵ superscript) methods. Circles show values obtained by the stress method, and squares by the strain method.

the PES at zero biaxial strain $e_{11}^h = e_{22}^h$ and zero normal strain e_{33}^h yielding $-2p_{11} = -2p_{22}$ and $-p_{33}$. The strain method is to find the strains $\epsilon_{11}^h = \epsilon_{22}^h$ and ϵ_{33}^h at the minimum of the PES. Setting $p_{ij} = V c_{ijkl} \epsilon_{kl}^h$ we obtain $p_{11} = p_{22} = V [(c_{11} + c_{12})\epsilon_{11}^h + c_{13}\epsilon_{33}^h]$ and $p_{33} = V [2c_{13}\epsilon_{11}^h + c_{33}\epsilon_{33}^h]$.

As the simulation cell increases in size the signal to noise ratio decreases owing to the larger number of small residual random forces on all atoms. In addition, the small but finite tolerance on the minimization of the electronic energy, and the \mathbf{k} -point sampling, lead to numerical errors in the predicted lattice constants of pure Zr in simulation cells of different sizes, which generate small

Zr atoms	Supercell	k-point grid	a (Å)	c (Å)	$c_{11} + c_{12}$ (GPa)	c_{33} (GPa)	ΔH_{H} (eV)	Ω_{H} (Å ³)
2(PBE)	$1a \times 1a \times 1c$	$12 \times 12 \times 6$	3.24056(2)	5.18235(6)	217.9(6)	175(1)		
2(LDA)	$1a \times 1a \times 1c$	$12 \times 12 \times 6$	3.1628(1)	5.0732(5)	223(2)	173(3)		
96(PBE)	$4a \times 4a \times 3c$	$3 \times 3 \times 2$	3.2422(2)	5.1818(7)	219(2)	172(5)	-0.46	3.26
150(PBE)	$5a \times 5a \times 3c$	$3 \times 3 \times 2$	3.23955(7)	5.1877(4)	217(1)	171(2)	-0.43	3.72
200(PBE)	$5a \times 5a \times 4c$	$3 \times 3 \times 2$	3.23889(7)	5.1844(3)	206(1)	172(3)	-0.43	3.23
288(PBE)	$6a \times 6a \times 4c$	$2 \times 2 \times 2$	3.2442(3)	5.173(1)	222(8)	169(15)	-0.46	3.39
392(PBE)	$7a \times 7a \times 4c$	$2 \times 2 \times 2$	3.24056(9)	5.1836(4)	201(1)	165(4)	-0.44	3.5
Exp.			3.226 ^(a)	5.130 ^(a)	223 ^(b)	173 ^(b)	-0.66 ^(c)	2.78 ^(d)

TABLE I: Parameters used for supercells and some results. Columns are: number of Zr atoms in each supercell, size of supercell in real space, k-point grids, optimal lattice parameters calculated for each supercell of pure Zr, calculated elastic constants of pure Zr, calculated solution enthalpy and formation volume of hydrogen in Zr. Estimated errorbars for lattice constants and elastic constants are in parentheses. Experimental data from (a) measurements at 300K [26] extrapolated to 0K using thermal expansion coefficients in [27], (b) measurements at 4K in [28], (c) [29], (d) [3].

stresses in the system before H is introduced. To quantify these errors we employed a boot-strapping method[20]. We randomly removed 13 of the 25 strain configurations and fitted a paraboloid through the remaining 12 DFT total energies. Repeating this procedure 100 times we determined the standard deviation of the strains that minimize the total energy of the supercells containing H, and the resulting standard deviation of the elastic dipole tensor is used as its errorbar.

For the defect forces method, the sum in Eq. (4) did not converge in the 96-atom supercell, but converged values within the errorbars of the simulations were obtained in the larger supercells. The results are displayed in Fig. 1a for both PBE and LDA functionals, together with the values deduced from experiment. The larger errorbars in the 392-atom supercell prevent refinement of the dipole tensor components deduced for smaller supercells. Taking the average of the dipole tensor components in the 150, 200, 288 and 392-atom supercells computed with the PBE functional we obtain for the defect forces method $p_{11} = 1.92 \pm 0.12$ eV and $p_{33} = 2.99 \pm 0.12$ eV.

The dipole tensor components obtained by the stress and strain methods using the PBE functional are shown in Fig. 1b. For the three smaller supercell sizes the circles and squares of a given color are quite close to each other, indicating reasonable agreement between the stress and strain methods. We note the errorbars do not vary systematically with supercell size, and they are not identical for both components of the dipole tensor. Using the stress method we obtain the following components of the dipole tensor: $p_{11} = 2.22 \pm 0.10$ eV, $p_{33} = 3.22 \pm 0.16$ eV. The components derived using the strain method are $p_{11} = 1.66 \pm 0.11$ eV, $p_{33} = 3.66 \pm 0.15$ eV.

We may use the strain method to evaluate the λ -tensor for direct comparison with the experimentally measured components, $\lambda_{11} = 0.033$ and $\lambda_{33} = 0.054$. We obtain $\lambda_{11} = 0.034 \pm 0.003$ and $\lambda_{33} = 0.069 \pm 0.007$. Domain et al. [6] obtained $\lambda_{11} = 0.033$ and $\lambda_{33} = 0.100$. Using

our calculated values of λ_{11} and λ_{33} , and the same elastic constants and lattice parameters as were used to calculate p_{11} and p_{33} from the experimental values of λ_{11} and λ_{33} (see the Supplemental Materials for details), we obtain $p_{11} = 1.74 \pm 0.12$ eV and $p_{33} = 2.36 \pm 0.18$ eV. These are the most reliable estimates of the dipole tensor because they use experimentally determined elastic constants and lattice parameters in combination with the calculated λ -tensor. We call this the λ -tensor method.

It is seen in Table I, and in ref.[6], that the structural and elastic properties of pure α -Zr are reproduced quite well by DFT with the PBE functional. The heat of solution is smaller and Ω_{H} is larger than experimental data in Table I. Domain et al. [6] obtained $\Delta H_{\text{H}} = -0.60$ eV and $\Omega_{\text{H}} = 3.9$ Å³, whereas Burr *et al.* [24] obtained $\Delta H_{\text{H}} = -0.46$ eV using CASTEP 5.5 [25], which agrees well with calculated values of ΔH_{H} in Table I using VASP.

Based on the work of MacEwen *et al.* [3], the errors in the experimental measurements of the λ -tensor are about $\pm 10\%$. Whereas the experimental and calculated values of λ_{11} are within the errors of the experiment and the calculation, the calculated value of λ_{33} is too large. There are possible sources of systematic error in the theory and the experiment. The sensitivity of the calculated dipole tensor components to the exchange-correlation functional is evident from the large differences between the PBE and LDA results in Fig 1a. In the experiment [3] it is possible that some D was not in solution but trapped at defects such as dislocations and grain boundaries, even though the experiments were undertaken at elevated temperatures. This would lead to an underestimate of the measured components of the λ -tensor and hence of the dipole tensor. However, it would not affect the experimentally measured ratio $\lambda_{33}/\lambda_{11} = 1.64 \pm 0.33$. The range of calculated values of $\lambda_{33}/\lambda_{11} = 2.03 \pm 0.40$ overlaps with the range of experimental values.

We suggest the overestimates of λ_{33} and Ω_{H} and the

underestimate of the magnitude of ΔH_{H} , in comparison with experimental measurements, are consistent with an underestimate of the attractive interaction between H and Zr-atoms along the c -axis of α -Zr in PBE-DFT.

In conclusion, the λ -tensor method provides the most accurate calculations of the dipole tensor: $p_{11} = 1.74 \pm 0.12$ eV and $p_{33} = 2.36 \pm 0.18$ eV. These are 10 – 20% higher than the values, $p_{11} = 1.57 \pm 0.11$ eV and $p_{33} = 1.96 \pm 0.14$ eV, deduced from the experimental measurement of the λ -tensor. The source of the overestimates for

p_{11} and p_{33} is the excessive calculated value of λ_{33} . DFT calculations of the dipole tensor using the defect forces method, stress method and strain method are prone to large numerical errors.

Work by R. N. was performed under the auspices of the U.S. Department of Energy by Lawrence Livermore National Laboratory under Contract No. DE-AC52-07NA27344. J. S. M and M. P. were supported by the EPSRC Centre for Doctoral Training on Theory and Simulation of Materials funded through EP/G036888/1. M. P. also received support from Rolls-Royce plc.

-
- [1] J. D. Eshelby in *The physics of metals* **2**, ed. P. B. Hirsch, p.1 Cambridge University Press: New York (1975).
- [2] G. Leibfried and N. Breuer in *Point defects in metals I*, p. 146 Springer-Verlag: New York (1978).
- [3] S. R. MacEwen, C. E. Coleman, C. E. Ells and J. Faber Jr. *Acta Metallurgica* **33**, 753 (1985).
- [4] M. P. Puls. *The Effect of Hydrogen and Hydrides on the Integrity of Zirconium Alloy Components: Delayed Hydride Cracking*. Springer: New York (2012).
- [5] P. P. Narang, G. L. Paul and K. N. R. Taylor. *J. Less Common Metals* **56**, 125 (1977).
- [6] C. Domain, R. Besson, and R. Legris. *Acta Mater.* **50**, 3513 (2002).
- [7] M. J. Gillan. *J. Phys. C: Sol. Stat. Phys.* **17**, 1473 (1984).
- [8] A. M. Stoneham, *Theory of defects in solids* p.166, OUP: Oxford (1975).
- [9] E. Clouet, S. Garruchet, H. Nguyen, M. Perez and C. Becquart. *Acta Mater.* **56**, 3450 (2008).
- [10] A. S. Nowick and B. S. Berry, *Anelastic relaxation in crystalline solid*, Academic Press: New York (1972).
- [11] G. Kresse and J. Hafner, *Phys. Rev. B* **47**, 558 (1993). G. Kresse and J. Hafner, *Phys. Rev. B* **49**, 14251 (1994). G. Kresse and J. Furthmüller, *Comput. Mat. Sci.* **6**, 15 (1996). G. Kresse and J. Furthmüller, *Phys. Rev. B* **54** 11169 (1996).
- [12] D. M. Ceperley and B. J. Alder, *Phys. Rev. Letts.* **45**, 566 (1980).
- [13] J. P. Perdew and A. Zunger, *Phys. Rev. B* **23**, 5048 (1981).
- [14] J. P. Perdew, K. Burke, M. Ernzerhof, *Phys. Rev. Lett.* **77** 3865 (1996); J. P. Perdew, K. Burke, M. Ernzerhof, *Phys. Rev. Lett.* **78**, 1396(E) (1997).
- [15] P. E. Blöchl. *Phys. Rev. B* **50**, 24 17953 (1994).
- [16] G. Kresse and D. Joubert. *Phys. Rev. B* **59**, 1758 (1999).
- [17] M. Methfessel and A. T. Paxton. *Phys. Rev. B* **40** 3616 (1989).
- [18] H. J. Monkhorst and J. D. Pack. *Phys. Rev. B* **13**, 5188 (1976).
- [19] R. Nazarov, T. Hickel, and J. Neugebauer, *Phys. Rev. B* **89**, 144108 (2014).
- [20] B. Efron and R. Tibshirani, *An Introduction to the Bootstrap*, Chapman & Hall/CRC, Boca Raton, Florida (1993).
- [21] K. Carling, G. Wahnström, T. R. Mattsson, A. E. Mattsson, N. Sandberg, and G. Grimvall, *Phys. Rev. Lett.* **85**, 3862 (2000).
- [22] T. R. Mattsson and A. E. Mattsson, *Phys. Rev. B* **66**, 214110 (2002).
- [23] R. Nazarov, T. Hickel, and J. Neugebauer, *Phys. Rev. B* **85** 144118 (2012).
- [24] P. A. Burr, S. T. Murphy, S. C. Lumley, M. R. Wenman and R. W. Grimes. *Corrosion Science* **69**, 1 (2013).
- [25] S. J. Clark, M. D. Segall, C. J. Pickard, P. J. Hasnip, M. J. Probert, K. Refson, M. C. Payne, *Z. Kristall.* **220**, 567 (2005).
- [26] B.D. Lichter, *Trans. Am. Inst. Min. Engrs.* **218**, 1015 (1960).
- [27] G. B. Skinner and H. L. Johnston, *J. Chem. Phys.* **21**, 1383 (1953).
- [28] E. S. Fisher and C J Renken, *Phys. Rev.* **135**, A482 (1964).
- [29] Y. Fukai *The metal-hydrogen system*, Springer: Berlin (2005).
- [30] H. R. Schober and K. W. Ingle, *J. Phys. F: Metal. Phys.* **10**, 575 (1980).
- [31] A. M. Monti, *Phys. Stat. Sol. (b)* **168**, 49 (1991).
- [32] A. Mallo and U. Yxklinten, *Z. Phys. B - Cond. Matter* **83**, 213 (1991).
- [33] G. Simonelli, R. Pasianot and E. J. Savino, *Phys. Rev. B* **50**, 727 (1994).
- [34] C. Domain and C. S. Becquart, *Phys. Rev. B* **65**, 024103 (2001).
- [35] D. Seif and N. M. Ghoniem, DOE/ER-0313/47 - Vol. 47. Semiannual Progress Report (2009) 113.
- [36] M. Leslie and M. J. Gillan, *J. Phys. C: Solid State Phys.* **18**, 973 (1985).
- [37] D. A. Freedman, D. Roundy and T. A. Arias. *Phys. Rev. B* **80**, 064108 (2009).
- [38] A. Vattre et al., *Nature Commun.* **7**, 10424 (2016).